TRAJECTORY RECONSTRUCTION OF A MARTIAN PLANETARY PROBE MISSION: RECONSTRUCTION OF THE SPIRIT MARS EXPLORATION ROVER ENTRY, DESCENT, AND LANDING PERFORMANCE

Grant WELLS - Guggenheim School of Aerospace Engineering, Georgia Institute of Technology, Atlanta, Georgia, USA
Dr. Robert BRAUN - Guggenheim School of Aerospace Engineering, Georgia Institute of Technology, Atlanta, Georgia, USA

ABSTRACT

Accurate post-flight reconstruction of a vehicle's trajectory during entry into a planetary atmosphere can produce a wide array of valuable information. Data collected through the reconstruction of entry, descent, and landing system performance enables the quantification of performance margins for future systems. Beyond the engineering knowledge gained through trajectory reconstruction, the results may also be used by planetary scientists to generate an accurate atmospheric profile. This paper provides a reconstruction of the trajectory, vehicle orientation, and atmospheric density profile for the hypersonic and supersonic phases of the Spirit Mars Exploration Rover spacecraft.

INTRODUCTION

Spirit

As part of the Mars Exploration Rover (MER) mission, the Spirit (MER A) spacecraft was launched on 10 June 2003. On 4 January 2004, Spirit landed in Gusev Crater (14.5°S, 175°E) on Mars.[1] Spirit's entry, descent, and landing (EDL) sequence was similar to that used for the Mars Pathfinder mission.[2] The spacecraft decelerated with its aeroshell and heatshield, then deployed a supersonic parachute, jettisoned its heatshield, and used retrorockets to minimize its velocity above the surface of Mars. The lander was then separated from the backshell and dropped to the surface protected by airbags. Once the motion of the lander ceased, the Spirit rover was deployed to make in situ science measurements.

Accelerometer Data

The Spirit spacecraft was equipped with two Litton LN-200S inertial measurement units (IMUs). One IMU was located in the backshell of the spacecraft's aeroshell, and the other IMU was located in the rover.[3] Both IMUs include 3-axis accelerometers and gyroscopes. The data obtained by the IMUs has been archived in the NASA Planetary Data System.[4] The IMUs have a dynamical range of 80 g_n (g_n = 9.80665 m/s^2) with a 2.4 mg_n, resolution, and noise levels of 1.6 mg_n. The MER IMUs obtained measurements at a frequency of 400 Hz. This data rate produced more data than the spacecraft could effectively use, so the IMU data was summed yielding measurements at an effective frequency of 8 Hz. This change in the effective data rate reduced the effective noise to 300 μg_n.[3] In comparison, the effective noise for the Mars Pathfinder mission accelerometers was less than 5 mg_n [5].

The Planetary Data System contains acceleration data for Spirit's backshell IMU and velocity change data for Spirit's rover IMU.[4] The backshell IMU accelerometer data was used in this investigation. The Spirit IMU output was converted on-board the spacecraft into physical units. The accelerations were transformed to the center of mass and into the spacecraft coordinate system based on the nominal (not measured) properties of the spacecraft.[4]

IMU output processing was performed on the spacecraft for all of the 8 Hz measurements. Due to memory limitations on-board the spacecraft, the frequency of the saved data varied depending on the EDL phase. Some of the transformed data was transmitted to Mars Global Surveyor during the EDL

sequence. The radio link between Spirit and Mars Global Surveyor was somewhat intermittent due to the relative motion of the spacecraft and the real-time nature of the data transmission. The interrupted communication caused some of this data to be lost. Fortunately, the data returned during entry, descent, and landing and the stored data sent back after landing are complementary in many cases. Specifically for Spirit, the two data streams were both at 4 Hz, but on alternating 8 Hz timesteps, which resulted in an effective 8 Hz data set (minus the data lost over the radio link).[4]

Post-flight analysis demonstrated that the y-axis acceleration was rotated by 0.31528° and the x-axis acceleration was rotated by 0.10886° relative to the principle body axes.[6] These values were determined such that the attitude oscillation was centered on 0° (no bias in the mean normal acceleration signals) for the oscillations near the parachute deployment condition. The total rotation of the backshell IMU axes was 1/3°.[6]

METHODOLOGY & RESULTS

Entry Conditions and EDL Timeline

The entry conditions and the properties of the Spirit spacecraft were compiled from several sources and are listed in Table 1. A timeline of EDL events is listed in Table 2.

Table 1: Best estimated entry conditions and properties of the Spirit spacecraft.

Parameter	Value	Source
Arrival Date	4 January 2004	[8]
Arrival Season	Winter	[8]
Local Time of Day at Landing Site	Approximately 2:00 p.m.	[7]
Landing Site Radius	3392.330 km	[7]
Landing Site Location	14.571892°S, 175.47848°E	[7]
Entry Direction	Posigrade	[8]
Entry Radius	3522.2 km ± 0.2087 km*	[7]
Inertial Entry Velocity	5.628 km/s ± 0.000046 km/s	[6,7]
Relative Entry Velocity	5.399 km/s	[6]
Inertial Entry Flight Path Angle	-11.4949178° ± 0.01°	[7]
Inertial Azimuth	79.0252068° ± 0.003°	[7]
Areocentric Entry Latitude	-17.7419926° ± 0.0032°*	[7]
Areocentric Entry Longitude	161.776543° ± 0.0172°*	[7]
Entry Mass	827 kg	[8]
Heatshield Mass	89.6 kg	[9]
Aeroshell Diameter	2.65 m	[10]
Parachute Diameter	14.1 m	[12]

*Uncertainties are based on an entry time error of 0.186 s.[7]

Table 2: A timeline of EDL events for the Spirit spacecraft.[13]

Event	Time after Entry (s)
Parachute Deployment	251[a]
Heatshield Jettison	271[a]
Retrorocket Firing Initiated	339.4[a]
Parachute Bridle Cut	348.2[b]
Landing	350.5[b]

[a]Reconstructed.[13]
[b]Mean value obtained from a simulation.[13]

Angle of Attack History

As shown previously for reconstructing the trajectory of Mars Pathfinder [14, 15, 16], the total angle of attack can be found using the accelerometer data, the following equations, and an aerodynamic database for the entry vehicle [18]. The normal and axial accelerations can be computed as:

$$a_N = \sqrt{a_x^2 + a_y^2} \tag{1}$$

$$a_A = a_z \tag{2}$$

where a_x, a_y, a_z (= a_A) are the accelerations along the body axes of the spacecraft, a_A is the axial acceleration, and a_N is the normal acceleration. The ratio of the normal to the axial aerodynamic force coefficient can be computed as:

$$\frac{C_N}{C_A} = \frac{\left(\dfrac{F_N}{\frac{1}{2}\rho v^2 S}\right)}{\left(\dfrac{F_A}{\frac{1}{2}\rho v^2 S}\right)} = \frac{ma_N}{ma_A} = \frac{a_N}{a_A} = \frac{a_N}{a_z} \tag{3}$$

where C_N and C_A are the normal and axial aerodynamic force coefficients, F_N and F_A are the normal and axial forces, ρ is the atmospheric density, v is the spacecraft relative velocity, S is the aerodynamic reference area, and m is the mass of the spacecraft.

Based on the accelerometer data, a time history of Spirit's total angle of attack can be estimated and is shown in Figure 1 for the continuum hypersonic regime [1] up until the time of parachute deployment. The Mach number profile is shown in Figure 1, for reference, based on the subsequent velocity reconstruction. The pre-flight prediction of static instability at approximately Mach 16 is clearly shown in this data as is the significant damping present in the region of peak dynamic pressure. Pre-entry analysis of Spirit's angle of attack history predicted angle of attack discursions less than 3° over all flight regimes.[1] Figure 1 shows angle of attack discursions as large as 8° at the time of parachute deployment.

The larger angle of attack discursions are in agreement with a prior study of the Mars Exploration Rover angle of attack histories that used quaternion information from the IMUs.[19] Post-flight reconstruction revealed anomalistic disturbance torques during the entries of the Mars Exploration Rovers. Due to the accessibility of the remains of Opportunity's aeroshell, the Opportunity rover took pictures of its aeroshell on the surface. These photographs showed that portions of the aeroshell thermal blanket assembly still remained.[19] This blanket assembly was supposed to burn off very early in the entry. However, the thermal blanket design was carried over from the Mars Pathfinder mission, which experienced significantly more heating during entry due to Pathfinder's higher entry velocity.[8] This study estimated the aerodynamic torques that the thermal blanket remnants could have produced during the entries of the Mars Exploration Rovers. A comparison of two estimates of the aerodynamic torque perturbations (one extracted from telemetry data and the other from Mars surface photographs) showed exceptional agreement.[19]

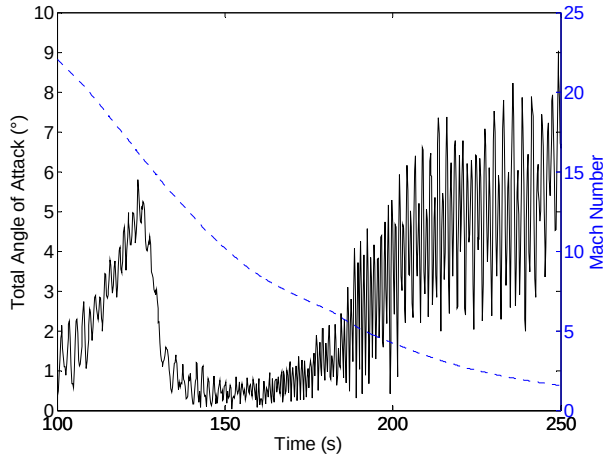

Figure 1: A time history of Spirit's total angle of attack and Mach number.

Atmospheric Density Profile

The angle of attack history and pre-flight aerodynamic database estimate was used to determine an atmospheric density profile at the time of Spirit's EDL with the use of Equation 4. This method has a long history in trajectory reconstruction but assumes perfect knowledge of C_A.[20, 14, 15, 16] The density profile is shown in Figure 2. There is good agreement between this estimate and a previous study as shown in Figure 3.

$$\rho = \frac{ma_A}{\frac{1}{2}v^2 SC_A} \tag{4}$$

A quadratic curve fit for the reconstructed atmospheric density profile is shown in Equation 5..

$$\begin{aligned}\rho = \exp(&-7.00870\times10^{-4}h^2 \\ &-3.69095\times10^{-2}h \\ &-4.75556)\end{aligned} \tag{5}$$

where the altitude (h) must be in kilometers, and the density is in kilograms per cubic meter.

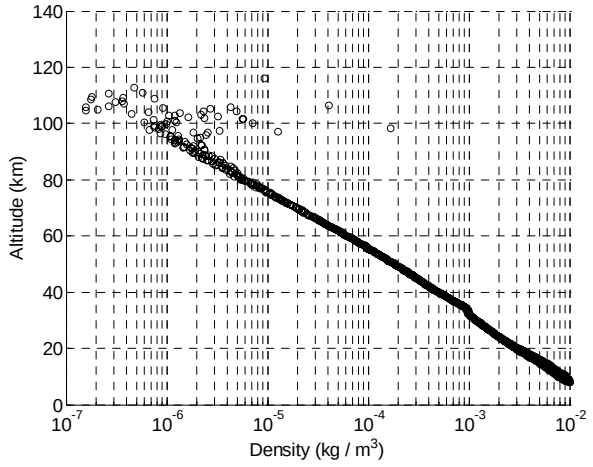

Figure 2: The reconstructed atmospheric density profile for Spirit's entry.

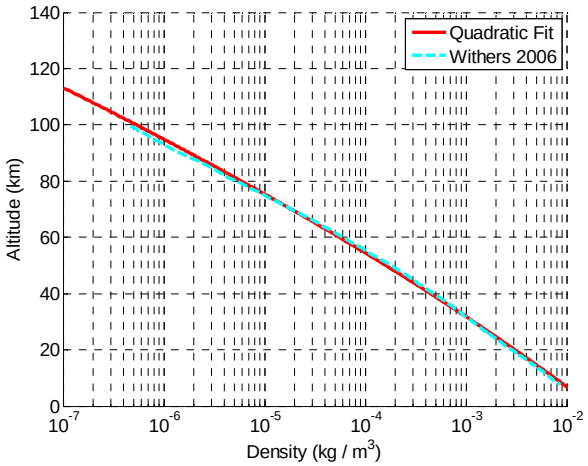

Figure 3: Comparison of the atmospheric density profile quadratic fit with Ref. [11].

The True, Nominal, & Best Estimate Trajectories

The true, nominal, and best estimate trajectories are related as shown in Figure 4. The true trajectory is not knowable since all uncertainty in the motion of the spacecraft cannot be eliminated. The best approximation of the true trajectory is the nominal trajectory. The nominal trajectory is created by modeling the motion of the spacecraft, and the best estimate trajectory can be determined by applying the extended Kalman filter to the nominal trajectory and the observations. As such, the best estimate trajectory does not rely on pre-flight models of the atmosphere.

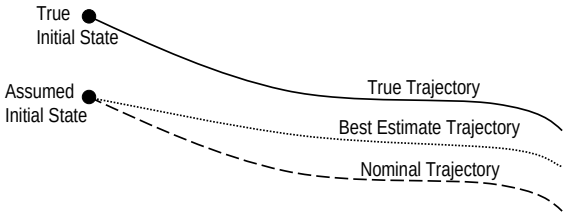

Figure 4: The true, nominal, and best estimate trajectories.

In this investigation, the best estimate trajectory for Spirit was generated using an extended Kalman filter and the backshell IMU accelerometer data. This extended Kalman filter has been used successfully for the reconstruction of the Mars Pathfinder trajectory.[14, 16] The theory and mathematics of the extended Kalman filter will not be discussed here. For details on extended Kalman filtering as applied to EDL trajectory reconstruction, the reader is directed to References [16] and [21].

Reconstructed Trajectory

Plots showing Spirit's reconstructed entry trajectory are provided in the following figures. Reconstruction is performed from the atmospheric interface (radius of 3522.2 km) to parachute bridle cut using a spherical gravity model. This trajectory reconstruction does not rely on pre-flight modeling of the atmosphere. Figure 5 shows the observed, nominal, and best estimate of the axial acceleration. Figure 6 shows the best estimate of the altitude-velocity curve. Figure 7 shows the best estimate of the velocity time history with 3-σ uncertainty bounds. Velocity uncertainty is quite small, approximately ±0.03 m/s at the time of parachute bridle cut. Figure 8 shows the best estimate of the altitude time history with 3-σ uncertainty bounds. At the time of parachute bridle cut, this uncertainty is approximately ±1.0 m.

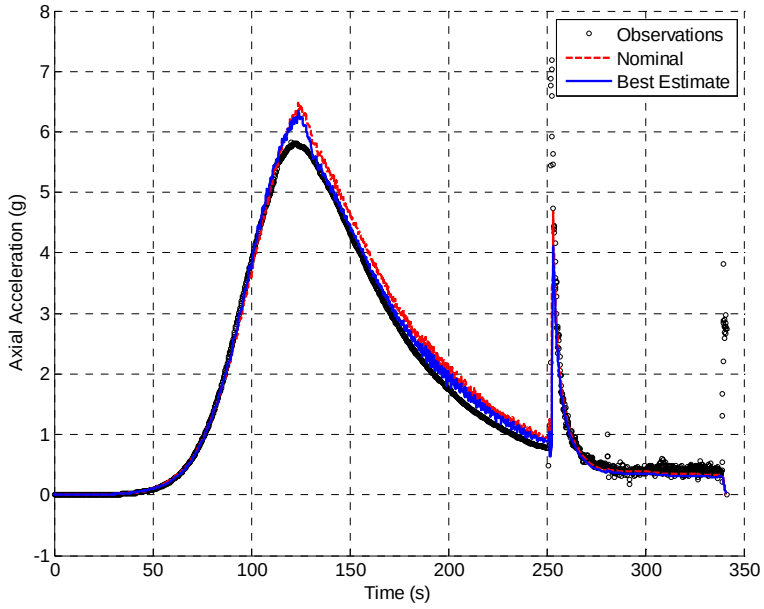

Figure 5: The observed, nominal, and best estimate axial accelerations.

For comparison, the Ref. [7] reconstruction, which incorporates other EDL measurements (e.g. radar altimeter data and the post-landed radiometric position estimate) is also shown in Figure 6, Figure 7, and Figure 8.

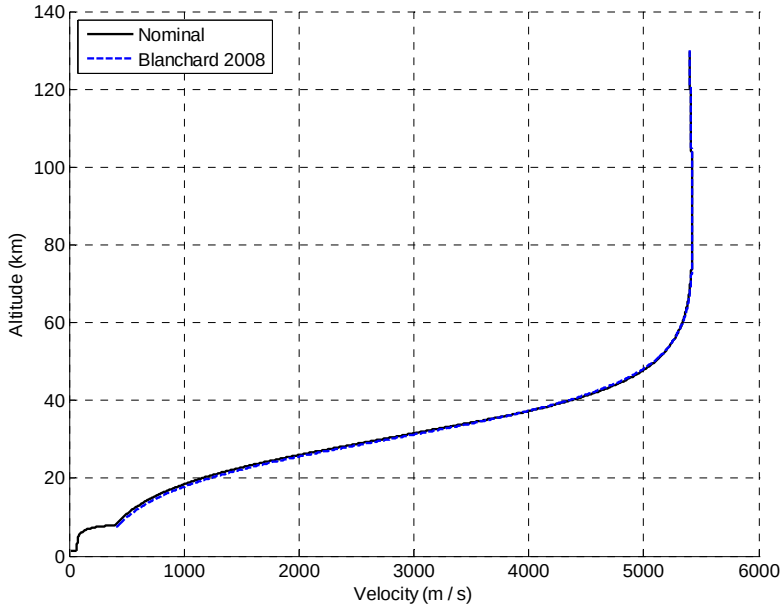

Figure 6: The best estimate altitude-velocity curve.

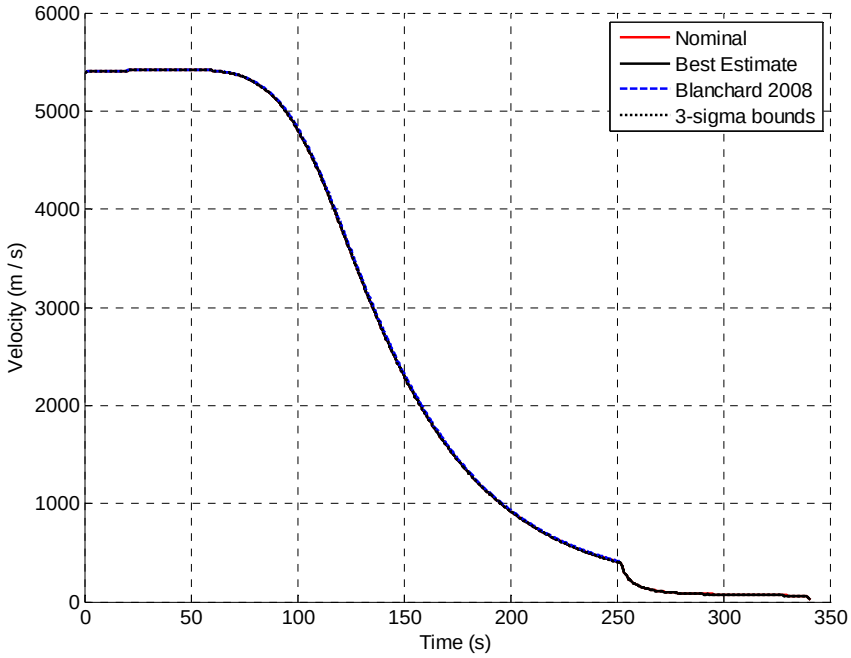

Figure 7: The best estimate of the velocity time history.

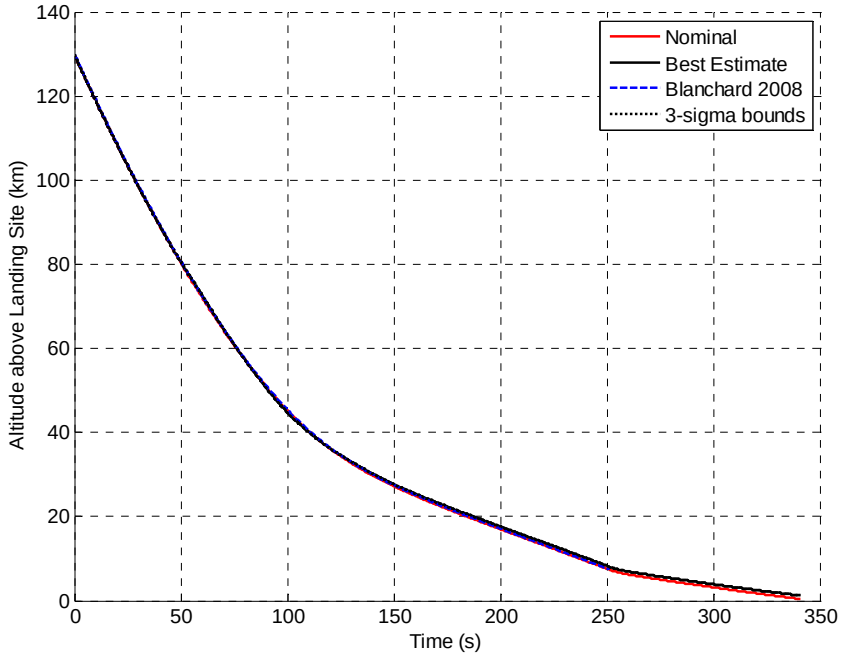

Figure 8: The best estimate altitude of the altitude time history.

Table 3 compares the pre-flight predictions of peak deceleration, velocity at parachute deployment, dynamic pressure at parachute deployment, and landed position with the best estimates from this investigation. Parachute deployment time was estimated based on locating the mortar deployment

acceleration in the backshell IMU data set. Table 4 compares the pre-flight EDL timeline of events with the reconstructed time of events from this investigation.

Table 3: A comparison of some pre-flight EDL parameters with best estimates.

Parameter	Pre-Flight Prediction	Pre-Flight Range	Best Estimate
Peak Deceleration (g)	5.9[a]	5.5 – 6.3[a]	6.3
Velocity at Parachute Deployment (m/s)	407[a]	377.5 – 436.5[a]	399
Dynamic Pressure at Parachute Deployment (Pa)	725.6[a]	654.8 – 796.3[a]	721.4
Landing Site Latitude	14.59°S[b]	5°N – 15°S[c]	14.51°S[d]
Landing Site Longitude	175.3°E[b]	-	175.4°E[d]

[a]From Ref. [13].
[b]From Ref. [22].
[c]From Ref. [23].
[d]Best estimate values of latitude and longitude are given at bridle cut since no backshell IMU data was recorded after bridle cut.

Table 4: A comparison of the pre-flight and reconstructed EDL timelines.

	Time after Entry (s)		
Event	Pre-Flight Mean[a]	Pre-Flight Range[a]	Reconstructed
Parachute Deployment	245.5	237.9 – 253.1	251
Heatshield Jettison	265.5	257.9 – 273.1	271[a]
Retrorocket Firing Initiated	346.7	317.3 – 376.2	339.2
Parachute Bridle Cut	349.7	320.6 – 378.7	341.2
Landing	352.3	322.9 – 381.5	-[b]

[a]From Ref. [13].
[b]No backshell IMU data was recorded after bridle cut.

CONCLUSIONS

A flexible trajectory reconstruction tool created for the reconstruction of the Mars Pathfinder mission trajectory has been successfully extended to the Mars Exploration Rover mission, demonstrating the tool's flexibility. The results of this reconstruction are consistent with those of other MER flight reconstruction analyses and the predicted pre-flight design performance.

REFERENCES

[1] P. Desai, M. Schoenenberger, F. Cheatwood, "Mars Exploration Rover Six-Degree-of-Freedom Entry Trajectory Analysis," *Journal of Spacecraft and Rockets*, Vol. 43, No. 5, pp. 1019-1025, September-October 2006.

[2] D. Spencer, R. Blanchard, R. Braun, P. Kallemeyn, S. Thurman, "Mars Pathfinder Entry, Descent, and Landing Reconstruction," *Journal of Spacecraft and Rockets*, Vol. 36, No. 3, pp. 357–366, May–June 1999.

[3] J. Crisp, M. Adler, J. Matijevic, S. Squyres, R. Arvidson, D. Kass, "Mars Exploration Rover Mission," *Journal of Geophys. Research - Planets*, Vol. 108, No. E12, 8061, doi:10.1029/2002JE002038, 2003.

[4] D. Kass, J. Schofield, J. Crisp, E. Bailey, E. Konefat, W. Lee, E. Litty, R. Manning, A. San Martin, J. Willis, R. Beebe, J. Murphy, L. Huber, MER1/MER2-M-IMU-4-EDL-V1.0, *NASA Planetary Data System*, 2004.

[5] J. Magalhães, J. Schofield, A. Seiff, "Results of the Mars Pathfinder Atmospheric Structure Investigation," *Journal of Geophysical Research - Planets*, Vol. 104, No. E4, pp. 8943–8955, 25 April 1999.

[6] M. Shoenenberger, "MER Flight Data," Personnel Correspondence with the Authors, 1 October 2008.

[7] R. Blanchard, "Entry Descent and Landing Trajectory and Atmosphere Reconstruction for the Mars Exploration Rovers Missions A and B," The George Washington University, Performed under NASA-JPL subcontract CCNS20568F, 15 April 2008 (white paper).

[8] P. Desai, P. Knocke, "Entry, Descent, and Landing Scenario for the Mars Exploration Rover Mission," *Journal of the Astronautical Sciences*, Vol. 55, No. 4, pp. 421-430, October-December 2007.

[9] B. Raiszadeh, E. Queen, "Mars Exploration Rover Terminal Descent Mission Modeling and Simulation," AAS-04-271, *Advances in the Astronautical Sciences*, Vol. 119, pp. 2661-2676, 2004.

[10] P. Desai, P. Knocke, "Mars Exploration Rovers Entry, Descent, and Landing Trajectory Analysis," *Journal of the Astronautical Sciences*, Vol. 55, No. 3, pp. 311-323, July-September 2007.

[11] P. Withers, M. Smith, "Atmospheric Entry Profiles from the Mars Exploration Rovers Spirit and Opportunity," *Icarus*, Vol. 185, No. 1, pp. 133-142, November 2006.

[12] A. Witkowski, R. Bruno, "Mars Exploration Rover Parachute System Performance," AIAA-2003-2100, *17th AIAA Aerodynamic Decelerator Systems Technology Conference and Seminar*, Monterey, California, USA, 19-22 May 2003.

[13] P. Desai, P. Knocke, "Mars Exploration Rovers Entry, Descent, and Landing Trajectory Analysis," AIAA-2004-5092, *AIAA/AAS Astrodynamics Specialist Conference and Exhibit*, pp. 797-804, Providence, Rhode Island, 16-19 August 2004.

[14] D. Spencer, R. Blanchard, R. Braun, P. Kallemeyn, S. Thurman, "Mars Pathfinder Entry, Descent, and Landing Reconstruction," *Journal of Spacecraft and Rockets*, Vol. 36, No. 3, pp. 357-366, May-June 1999.

[15] P. Gnoffo, R. Braun, K. Weilmuenster, R. Mitcheltree, W. Engelund, R. Powell, "Prediction and Validation of Mars Pathfinder Hypersonic Aerodynamic Database," *Journal of Spacecraft and Rockets*, Vol. 36, No. 3, pp. 367-373, May-June 1999.

[16] J. Christian, A. Verges, and R. Braun, "Statistical Reconstruction of Mars Entry, Descent, and Landing Trajectories and Atmospheric Profiles," AIAA-2007-6192, *AIAA Space 2007 Conference and Exposition*, Long Beach, California, 18-20 September 2007.

[17] P. Gnoffo, K. Weilmuenster, R. Braun, C. Cruz, "Influence of Sonic-Line Location on Mars Pathfinder Probe Aerothermodynamics," *Journal of Spacecraft and Rockets*, Vol. 33, No. 2, pp. 169-177, March-April 1996.

[18] M. Schoenenberger, F. Cheatwood, P. Desai, "Static Aerodynamics of the Mars Exploration Rover Entry Capsule," AIAA-2005-56, *43rd AIAA Aerospace Sciences Meeting and Exhibit*, Reno, Nevada, 10-13 January 2005.

[19] R. Tolson, W. Willcockson, P. Desai, P. Thomas, "Anomalistic Disturbance Torques during the Entry Phase of the Mars Exploration Rover Missions - A Telemetry and Mars-Surface Investigation," AAS-06-087, *Advances in the Astronautical Sciences*, Vol. 125, pp. 507-525, 2006.

[20] A. Seiff, "Some Possibilities for Determining the Characteristics of the Atmospheres of Mars and Venus from Gas Dynamic Behavior of a Probe Vehicle," NASA TN-D-1770, April 1963.

[21] P. Desai, R. Blanchard, R. Powell, "Entry Trajectory and Atmosphere Reconstruction Methodologies for the Mars Exploration Rover Mission," European Space Agency Special Publication (ESA SP), No. 544, pp. 213-220, February 2004.

[22] P. Knocke, G. Wawrzyniak, B. Kennedy and M. Golombek, P. Desai, T. Parker, "Mars Exploration Rovers Landing Dispersion Analysis," AIAA-2004-5093, *AIAA/AAS Astrodynamics Specialist Conference and Exhibit*, pp. 797-804, Providence, Rhode Island, 16-19 August 2004.

[23] A. Steltzner, W. Lee, R. Bruno, P. Desai, "The Mars Exploration Rovers Entry Descent and Landing Phase and the Use of Aerodynamic Decelerators," AIAA-2003-2125, *17th AIAA Aerodynamic Decelerator Systems Technology Conference and Seminar*, Monterey, California, 19-22 May 2003.